Biointerface Research in Applied Chemistry
Open-Access Journal (ISSN: 2069-5837)

Article
Volume 16, Issue 2, 2026, 61
https://doi.org/10.33263/BRIAC162.061

In Silico Evaluation of Fucoxanthin Derivatives as SCAP Inhibitors

Shivaleela Biradar [1,*], Murali Krishna Paidi [1], T. S. Keshava Prasad [1,*]

[1] Center for Systems Biology and Molecular Medicine [An ICMR -Collaborating Centre of Excellence 2024 (ICMR-CCoE 2024)], Yenepoya Research Center, Yenepoya (Deemed to be University), Mangalore 575018, India; shivaleelabiradar4@gmail.com (S.B.); 37996@yenepoya.edu.in (M.K.P.); keshav@yenepoya.edu.in (T.S.K.);
* Correspondence: keshav@yenepoya.edu.in (T.S.K.); 34525@yenepoya.edu.in (S.B.);

Received: 23.04.2025; Accepted: 27.07.2025; Published: 15.04.2026

Abstract: Fucoxanthin (FX) is a marine carotenoid from brown algae that is metabolized in the body into fucoxanthinol (FXOH) and amarouciaxanthin A (AXA). Previous studies state that FX exhibits strong antioxidant activity, reduces free fatty acid synthesis, and modulates lipid metabolism. However, its inhibitory potential on SREBP Cleavage-Activating Protein (SCAP) remains unexplored. This study employed *in silico* techniques to assess the binding efficiency of FX and its derivatives against SCAP, using fatostatin and UT-59 as reference inhibitors. ADME profiling revealed that all natural ligands were lipophilic and poorly water-soluble. Molecular docking showed that AXA had the strongest binding affinity (-7.543 kcal/mol), followed by UT-59 (-6.846 kcal/mol), fatostatin (-5.743 kcal/mol), FXOH (-4.853 kcal/mol), and FX (-4.175 kcal/mol). AXA formed a key hydrogen bond with residue A268 in the SCAP luminal domain. Molecular dynamics simulations over 100 ns confirmed stable protein-ligand interactions, with RMSD values ranging between 7.5 and 9 Å. MM-GBSA binding free energy for FX (-55.09 kcal/mol) and AXA (-35.86 kcal/mol) supported their favorable interactions. Fucoxanthin derivatives, especially AXA, demonstrate promising SCAP inhibitory potential and could be explored further for natural, cholesterol-lowering therapeutics. Further, *in vitro* and *in vivo* experimental validations are needed for natural drug formulation.

Keywords: cholesterol; fucoxanthin; fucoxanthinol; amarouciaxanthin A; SREBP cleavage-activating protein; docking; molecular dynamics simulation.

1. Introduction

Fucoxanthin (FX) is a xanthophyll carotenoid derived from marine brown algae. Marine brown algae include diatoms (Class: Bacillariophyceae) and brown seaweeds (Class: Dictyotaceae) [1–3]. FX has attracted significant attention due to its diverse biological activities, dietary benefits, and potential therapeutic applications [4]. An allenic link (C=C=C), a 5,6-monoepoxide, and a conjugated carbonyl group (C=O) are among the distinctive structural characteristics of fucoxanthin, contributing to its remarkable bioactivity [5,6]. Fucoxanthin exhibits antioxidant activity, primarily by scavenging free radicals and reactive oxygen species (ROS) and by enhancing endogenous antioxidant defense systems, making it a crucial physiological component [7–10]. Fucoxanthin reduces fat storage and enhances thermogenesis by raising energy expenditure through the upregulation of uncoupling protein 1

(UCP1) in white adipose tissue [11,12]. Its anti-obesity effect, one of its most studied properties, is partially due to its ability to regulate lipid metabolism [13,14]. An *in vivo* experimental study using a mouse model revealed that dietary supplementation with wakame (Edible seaweed; *Undaria pinnatifida*) lipids (WLs), rich in fucoxanthin, may improve insulin resistance and modulate lipid metabolism altered by a high-fat (HF) diet. These findings confirm that fucoxanthin-rich WLs serve as a functional meal to reduce diabetes and obesity-related conditions [15]. Additionally, dietary supplementation with FX dramatically lowers hepatic lipid levels in mice, increases fecal lipid excretion, and decreases plasma triglyceride concentrations [16].

Apart from its distinct biological effects, the metabolic derivatives of fucoxanthin in the human body enhance its bioactivity far more than its individual biological effects. When FX is administered orally to mice, it is deacetylated in the gastrointestinal system by either lipase or cholesterol esterase to produce its primary metabolite, fucoxanthinol (FXOH), which is subsequently de-epoxidized in the liver to produce amarouciaxanthin A (AXA). These metabolites have higher bioavailability and support the long-term biological effects of fucoxanthin, especially in lipid metabolism and anti-inflammatory reactions [17,18]. Cardiovascular health is improved by fucoxanthin, which also lowers cholesterol and decreases the production of arterial plaque. According to an *in vivo* investigation by Ha and Kim (2013), mice fed with a high-fat diet containing 0.2% fucoxanthin (HF+Fxn) for four weeks showed higher HDL levels, lower hepatic total lipids, cholesterol, and triglycerides, and higher excretion of these lipids in the feces as compared to the high-fat diet (HF) control group. Moreover, at the mRNA level, the HF+Fxn-treated group showed lower hepatic mRNA expression of Acetyl-CoA carboxylase (ACC), Glucose-6-phosphate dehydrogenase (G6PDH), Fatty acid synthase (FAS), and Sterol regulatory element-binding protein-1C (SREBP-1C), along with reduced expression of Hydroxy-3-methylglutaryl coenzyme A (HMG-CoA) reductase and Acyl-CoA cholesterol acyltransferase (ACAT), and an elevated expression of Lecithin-cholesterol acyltransferase (LCAT) [19]. Thus, fucoxanthin promotes lipid metabolism and cholesterol removal by suppressing HMG-CoA reductase and increasing the expression of LDL receptors, hence preventing atherosclerosis.

As studies progress, the bioactive potential of fucoxanthin and its derivatives is recognized for its important role in managing health and illness. In the current study, the chemical characteristics and inhibitory potential of fucoxanthin and its natural derivatives on SREBP Cleavage-Activating Protein (SCAP, also abbreviated in some articles as SREBP-Cap) are assessed by computational approaches. SCAP is an essential ER-resident cholesterol sensor and escort protein that regulates the activation of Sterol Regulatory Element-Binding Proteins (SREBPs), including SREBP-1c and SREBP-2. SCAP plays a critical role in cholesterol and lipid homeostasis by controlling the movement of SREBP precursors from the endoplasmic reticulum (ER) to the Golgi apparatus [20]. Under low sterol conditions, SCAP binds to SREBPs and transports them to the Golgi, where Site-1 Protease (S1P) and Site-2 Protease (S2P) cleave SREBP, releasing its active form of transcription factor. This mature SREBP then translocates to the nucleus and upregulates lipid biosynthesis genes. However, when cellular sterol levels are sufficient, SCAP interacts with insulin-induced gene-1/2 (Insig-1 or -2) proteins, retaining SREBPs in the ER and preventing their activation. Dysregulation of SCAP mediated SREBP activation contributes to metabolic disorders such as non-alcoholic fatty liver disease (NAFLD), obesity, and hyperlipidemia, making SCAP a potential therapeutic target for lipid-related diseases [21].

The lipophilicity, high membrane diffusion, and low bioavailability of fucoxanthin and its derivatives enhance their therapeutic potential for lipid metabolic and neurological disorders [22,23]. However, its binding affinity and interaction modes with SREBP cleavage-activating protein (SCAP) remain unclear. The current study employs *in silico* approaches to evaluate the potential of fucoxanthin and its derivatives as SCAP inhibitors by comparing their efficiency and specificity with the synthetic drugs fatostatin and UT-59. We hypothesize that fucoxanthin and its derivatives can regulate sterol biosynthesis by suppressing SCAP activity more efficiently than fatostatin and UT-59. This computational study explores fucoxanthin and its derivatives as potential SCAP inhibitors, offering a natural strategy for managing lipid-related metabolic disorders.

2. Materials and Methods

2.1. Structural characterization of SCAP.

The primary structure of the Sterol Regulatory Element-Binding Protein Cleavage-Activating Protein (SCAP) was predicted by the ProtParam server (https://web.expasy.org/protparam/) (Table S1). The physicochemical properties of the protein, including molecular weight, isoelectric point (pI), aliphatic index, instability index, grand average of hydropathicity (GRAVY) of the protein (Table S2), and secondary structure of the protein, were predicted through NetSurfP 3.0 [24] (Figure S1). The functional domain of the targeted protein is predicted through PROSITE [25] (Table S3).

2.2. Protein preparation for docking.

The human SCAP protein cryo-electron microscopy structure (PDB ID: 7ETW) was retrieved from the Protein Data Bank (PDB, https://www.rcsb.org/). The 3-dimensional structure has a resolution of 4.10 Å. Before docking, the retrieved protein structure was prepared in the preparation wizard by adding hydrogen atoms, filling missing side chains, assigning bond orders, generating states with Epik, and reconstructing missing loops with Prime. Protein chains were reviewed and optimized, the structure was reviewed, crystallographic water molecules were removed, and disulfide bonds were created. Then, constrained minimization was performed using the impact refinement module with the PLS4 force field to optimize the protein shape and reduce its energy [26].

2.3. Active site prediction and grid generation.

The Sitemap module was used to anticipate the SCAP active site [27]. The active site with the highest site score, D-score (Druggability score), and size was selected. The Receptor Grid Generation module was utilized to produce active site coordinates using the Receptor Grid Generation, which was employed through the default right-handed Cartesian coordinate system. In grid generation, the van der Waals radii scaling was set to 1.0, the partial charge cutoff was set to 0.25, and the remaining parameters were kept in default settings as per Schrödinger (Schrödinger 2024-4). Thereafter, the Glide docking module was used for molecular docking experiments to assess ligand interactions inside the anticipated active site [28].

2.4. Ligand preparation.

The marine xanthophyll compounds, such as fucoxanthin and its derivatives, were selected as ligands to evaluate their potential to inhibit SCAP and reduce cholesterol synthesis. Publicly available SDF files of ligands were retrieved from the PubChem database (Figure 1). Ligand preparation was performed using the LigPrep module [29] with the following options: i) applied OPLS4 force field; ii) ionization generation with possible states at a target pH between 7±2 via Epik Classic; iii) stereoisomer computation was performed to retain the specified chirality of ligands. Moreover, Absorption, Distribution, Metabolism, and Excretion (ADME) properties were predicted through the QikProp module [30]. The toxicity of each ligand was predicted through the ProTox-3.0 server [31]. Subsequently, well-known SCAP inhibitory synthetic drugs such as fatostatin and UT-59 were used as a reference control to compare the inhibition potential of fucoxanthin and its derivatives.

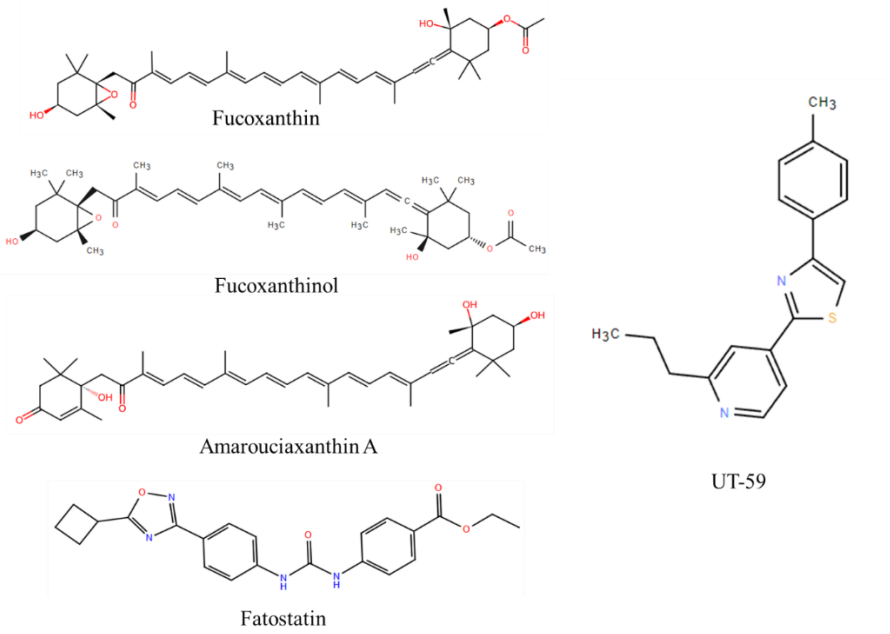

Figure 1. Chemical structure of fucoxanthin and its natural derivatives (Fucoxanthinol and Amarouciaxanthin A), reference drugs (Fatostatin and UT-59).

2.5. Identification of SCAP inhibitor using the glide module.

Molecular Docking (MD) was performed to identify an effective active fucoxanthin derivative that had the potential to inhibit the SCAP protein. Docking was employed using the Glide docking method in standard precision (SP) to evaluate the ligand binding score. Glide docking was performed using pre-processed protein and ligand output files from the protein and ligand preparation processes [28]. Ligand binding poses were assessed based on docking scores and the best pose for further interaction analysis, binding affinity, and molecular dynamics simulation studies.

2.6. Evaluation of protein-ligand dynamics stability.

The stability of the selected fucoxanthin derivatives in the SCAP binding site was assessed using the Desmond module in Schrödinger viaolecular dynamics simulation (MDS) for 100 ns [32]. To neutralize the system, counterions were introduced after the protein-ligand combination was put in a TIP3P water box with periodic boundary conditions. The OPLS4

force field was used to minimize and equilibrate the system [33]. The NPT ensemble was used to do simulations with a time step of 2 fs at 300 K and 1 atom. While performing simulations, the stability of the protein-ligand complex was evaluated using Root Mean Square Deviation (RMSD) trajectory analysis. The stability of the ligand within the binding pocket was evaluated by creating an RMSD plot for the protein-ligand complex's backbone atoms. Maestro 14.2 version (Schrödinger 2024-4) was utilized for the analysis and visualization of the SCAP-inhibitor complex.

2.7. Prediction of MM-GBSA.

To calculate the binding free energy (ΔG bind) of ligand molecules through the Molecular Mechanics Generalized Born Surface Area (MM-GBSA) method [34], the Schrödinger suite module's OPLS4 force field was used for the main MM-GBSA computation involving the ΔG bind between protein and ligand complexes. The primary MM-GBSA technique was used to determine the ΔG bind of each selected ligand. The G ratings were then applied to the top compounds that were extracted from the docking pathway. The protein-ligand complexes' ΔG binding was determined using the MM-GBSA analysis included in the GLIDE Prime module [35].

$\Delta G_{binding}$ was calculated based on the following formula:

$$\Delta G_{binding} = Energy\ of\ the\ minimized\ complex\ - (Energy\ of\ the\ minimized\ ligand\ +\ Energy\ of\ the\ minimized\ receptor) \quad (1)$$

3. Results

3.1. Structural characterization of SCAP.

The targeted protein SCAP comprises 1279 amino acids with an isoelectric point (pI) of 6.41. Its primary structure, amino acid composition, and physicochemical properties were illustrated in Tables S1 and S2. The isoelectric point (pI 6.41) suggests that SCAP was slightly acidic. An instability index of 53.68 indicates its instability, whereas a high aliphatic index of 97.31 represents thermostability. A positive GRAVY value (0.022) represents SCAP containing more non-polar residues. The secondary structure of the protein SCAP was presented in Figure S1, illustrating α-helix, β-sheets, turns, and coils. The α-helices were represented in orange, β-strands in blue, and the coils in pink. Relative surface accessibility was represented as follows: red indicates exposed regions, blue denotes buried regions with a 20% threshold, and grey indicates disorder regions. The thickness of the line equals the probability of disordered residues. The PROSITE domain analysis identified three functional domains (i.e., PS50156, PS50294, PS50082) in the SCAP protein. Out of three, the PS50156 domain was the most conserved and had the highest score (43.285) (Table S3). After reviewing all properties, the protein's three-dimensional (3D) structure was downloaded, and the active site was predicted in the luminal domain of SCAP using the sitemap module (Figure 2). The site was selected based on the highest Dscore and Site score (Dscore: 1.123 & SiteScore: 1.079) of sitemap results. Based on these results, the receptor grid generation module was used to develop the grid for the targeted protein. Further Glide was used in molecular docking studies with the extra precision (XP) method.

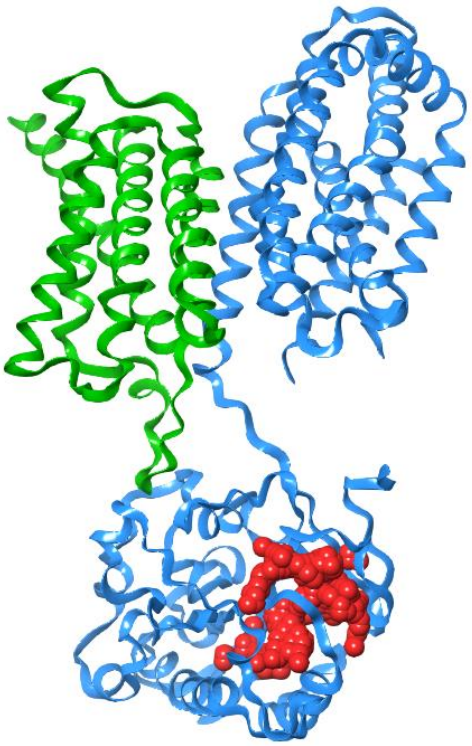

Figure 2. Active site of the SCAP protein predicted using Sitemap, shown as red ball-like structures.

3.2. Drug-likeness, ADME, and toxicity analysis.

3.2.1. Drug-likeness.

The drug-like properties of fucoxanthin, its derivatives, and reference compounds are presented in Table 1. Drug-likeness is determined by several factors, such as polar surface area (7.0 – 200.0), H-bond donors (0.0 – 6.0), H-bond acceptors (2.0 – 20.0), projected octanol/water partition coefficient (−2.0 – 6.5), and molecular weight (130 - 725). The ligands that were chosen in this study showed satisfactory pharmacophore characteristics, except variations in the anticipated values of the octanol/water partition coefficient (QPlogPo/w).

Table 1. Drug likeness property of the compounds.

Compounds	Fucoxanthin	Fucoxanthinol	Amarouciaxanthin A	Fatostatin	UT-59
MW	658.917	616.879	614.864	294.414	406.440
$QplogP_{o/w}$	9.860	8.917	9.096	5.194	3.171
donorHB	1	2	2	0	2
accptHB	7.450	7.150	6.200	2.500	7.000
PSA	110.798	96.643	106.592	21.589	119.599

[1]MW: Molecular weight (130 to 725), QplogPo/w: Predicted octanol/water partition coefficient (−2.0 to 6.5), donorHB: H-bond donor (0.0 to 6.0), accptHB: H-bond acceptor (2.0 to 20.0), PSA: Polar Surface Area (7.0 to 200.0). The acceptable range of drug-likeness parameters as per QikProp (Schrödinger 2024-4).

3.2.2. ADME and toxicity analysis.

The ADME analysis of FX, FXOH, and AXA revealed favorable pharmacokinetic profiles, indicating good drug-likeness. These compounds exhibited acceptable absorption, distribution, and metabolic (ADME) properties, with no major violations of drug-likeness rules (Table 2). The predicted aqueous solubility level (QplogS) of FX, FXOH, and AXA showed (-12.274, -10.931, and -11.213) higher negativity as compared to the reference drugs fatostatin (-6.340) and UT-59 (-6.824). Similarly, the conformation-independent predicted aqueous solubility (CIQPlogS) also showed higher negativity for FX (-9.569), FXOH (-8.734), and

AXA (-9.394) than the reference drugs. From this observation, the FX, FXOH, and AXA have lower water solubility than fatostatin and UT-59. The drug permeability parameters, such as apparent gut-blood barrier permeability (QPPCaco), Skin permeability (QplogKp), Brain/blood partition coefficient (QplogBB), and IC50 value for blockage of hERGK+ channels (QPlogHERG), showed an acceptable range. Central nervous system activity for FX, FXOH, AXA, and UT-59 was less inactive (-2) than fatostatin (1). Similarly, transdermal absorption was poor as compared to fatostatin. From these findings, the FX, FXOH, and AXA exhibited low predicted BBB permeability, indicating limited potential for central nervous system (CNS) exposure. This may be advantageous in reducing the risk of CNS-related side effects. Despite the low BBB permeability, all three compounds demonstrated high gastrointestinal (GI) absorption, supporting their suitability for oral administration. Furthermore, no hepatotoxicity was predicted, suggesting a favorable safety profile. These pharmacokinetic properties support the potential of these fucoxanthin derivatives as effective and safe SCAP-targeting agents. These findings support their potential for further development as SCAP-targeting agents.

Table 2. Absorption, distribution, metabolism, and excretion (ADME) properties of the compounds.

Compounds	Fucoxanthin (FX)	Fucoxanthinol (FXOH)	Amarouciaxanthin A (AXA)	Fatostatin	UT-59
QplogS	-12.274	-10.931	-11.213	-6.340	-6.824
CIQPlogS	-9.569	-8.734	-9.394	-5.185	-4.762
QPPCaco	470.495	398.358	257.907	6230.163	160.961
#metab	7	8	10	4	1
CNS	-2	-2	-2	1	-2
QplogBB	-2.742	-2.763	-3.035	0.332	-1.777
QplogKp	-1.543	-1.691	-2.022	-0.694	-3.270
Jm	0	0	0	0.027	0
QPlogHERG	-7.211	-6.961	-7.014	-5.978	-5.774

2QplogS: Predicted aqueous solubility level (−6.5 to <0.5), CIQPlogS: Conformation-independent predicted aqueous solubility (−6.5 to 0.5), QPPCaco: Predicted apparent gut-blood barrier permeability (<25 = Poor, >500 = Great), #metab: Number of likely metabolic reaction (1 to 8), CNS: Central nervous system activity (−2 = Completely inactive, −1 = Very low activity, 0 = Low activity, 1 = Medium activity, 2 = Completely active), QplogBB: Predicted brain/blood partition coefficient (−3.0 to 1.2), QplogKp: Predicted skin permeability (−8 to −1), Jm: Predicted maximum transdermal transportrate, QPlogHERG: Predicted IC50 value for blockage of hERGK+ channels (concern below −5).

Toxicity parameters of FX, FXOH, and AXA were assessed and compared with reference drugs, and the results were summarised in Table 3. The toxicity prediction reveals that the oral consumption of amarouciaxanthin A (AXA), fatostatin, and UT-59 was less toxic than FX and FXOH. Fucoxanthin and its derivatives were predicted to be non-hepatotoxic, whereas the reference drugs showed mild hepatotoxicity. Additionally, all compounds were classified as non-toxic concerning neurotoxicity, mutagenicity, cytotoxicity, and cardiotoxicity. However, carcinogenicity was considered mildly active for FX, FXOH, and UT-59 compounds. From these observations, AXA demonstrated no toxicity across all toxicity parameters.

Table 3. Toxicity prediction of the compounds and reference drugs.

Toxicity parameters	Name of the compound				
	Fucoxanthin (FX)	Fucoxanthinol (FXOH)	Amarouciaxanthin A (AXA)	Fatostatin	UT-59
Predicted LD_{50}	130 mg/kg	130 mg/kg	900 mg/kg	1000 mg/kg	1000 mg/kg
Toxicity Class	3	3	4	4	4
Hepatotoxicity	Inactive	Inactive	Inactive	Mild-Active	Mild-Active

Toxicity parameters	Name of the compound				
	Fucoxanthin (FX)	Fucoxanthinol (FXOH)	Amarouciaxanthin A (AXA)	Fatostatin	UT-59
Neurotoxicity	Inactive	Inactive	Inactive	*Inactive*	Inactive
Carcinogenicity	Mild-Active	Mild-Active	Inactive	Inactive	Mild-Active
Mutagenicity	Inactive	Inactive	Inactive	*Inactive*	Inactive
Cytotoxicity	Inactive	Inactive	Inactive	Inactive	Inactive
Cardiotoxicity	Inactive	Inactive	Inactive	Inactive	Inactive

[3]LD_{50} – Lethal dose 50; mg/kg – Milligrams per kilogram; Toxicity class (1 to 6), 1 is toxic and 6 is non-toxic.

3.3. Protein-ligand binding interaction analysis.

The SREBP cleavage-activating protein (SCAP) is a transmembrane protein found in the endoplasmic reticulum (ER) membrane, where it is associated with Insulin-induced gene 1 or 2 (INSIG 2) to form the SCAP/INSIG complex. SCAP consists of two major segments: one is a cytosolic segment, and the other is a luminal segment. Sitemap analysis identified a potential binding pocket in the SCAP luminal segment. Moreover, protein-ligand docking analysis revealed interactions between SCAP and ligands (i.e., FX, FXOH, AXA, fatostatin, and UT-59), including docking scores, hydrogen bonds, and hydrophobic interactions; the forming residues were summarized in Table 4.

Table 4. Binding interaction analysis of the compounds and the reference drug, binding score, and hydrophobic interaction residues.

Compound	Docking Score (XP)	H-Bond	Hydrophobic Interaction
Fucoxanthin (FX)	-4.175	-	L148, V150, Y640, I642, A91, V90, P89, A88, Q241, H242, Y243, H244, A245, K246, E80, Q81, P82, E83, W84
Fucoxanthinol (FXOH)	-4.853	Y640	L148, V150, D152, F637, I642, R647, A91, V90, P89, A88, V86, W84, E83, P82, Q81, Q241, H242, Y243, H244, A245.
Amarouciaxanthin A (AXA)	-7.543	A268	V90, A88, G87, V86, W84, E83, P82, Q81, E80, L271, E269, L266, G249, R252, A245, Y243, H242, Q241.
Fatostatin	-5.743	-	Y92, V90, A88, G87, V86, W84, E83, P82, Q81, E80, Q241, H242, Y243, S650, L271
UT-59	-6.846	D136	L146, E145, L143, R141, S138, S137, L248, F247, H244, Y243, H242, F240, V239, L238, Y92, V93, Q94

Fucoxanthin exhibited a binding energy of -4.175 kcal/mol, and it was stabilized by hydrophobic interactions with L148, V150, Y640, I642, A91, V90, P89, A88, Q241, H242, Y243, H244, A245, K246, E80, Q81, P82, E83, W84 (Figure 3) within the active site of SCAP. Similarly, the binding energy of fucoxanthinol (FXOH) was -4.853 kcal/mol and formed an H-bond with the Y640 side chain at a distance of 2.43 Å. The hydrophobic interactions with residues of L148, V150, D152, F637, I642, R647, A91, V90, P89, A88, V86, W84, E83, P82, Q81, Q241, H242, Y243, H244, and A245 stabilize the binding of FXOH in the (Figure 4). Whereas, Amarouciaxanthin A (AXA) has -7.543 kcal/mol binding energy and forms a H-bond with the A268 side chain with a distance of 2.03 Å. The compound was stabilized by hydrophobic interactions with residues of V90, A88, G87, V86, W84, E83, P82, Q81, E80, L271, E269, L266, G249, R252, A245, Y243, H242, and Q241 in the binding site of SCAP (Figure 5). Fatostatin showed a binding energy of -5.743 kcal/mol, and it was stabilized through hydrophobic interactions with residues Y92, V90, A88, G87, V86, W84, E83, P82, Q81, E80, Q241, H242, Y243, S650, and L271 within the active site of SCAP (Figure 6). UT-59 exhibited -6.846 kcal/mol of binding energy and formed an H-bond with the D136 side chain at a distance of 2.02 Å. Additionally, its binding was reinforced by hydrophobic interactions involving L146, E145, L143, R141, S138, S137, L248, F247, H244, Y243, H242, F240, V239, L238, Y92, V93, Q94 (Figure 7). From these observations, Amarouciaxanthin A exhibited the highest

binding interaction (-7.543) with SCAP compared to FX (-4.175), FXOH (-4.853), fatostatin (-5.743), and UT-59 (-6.846). FX and fatostatin did not form hydrogen bonds with the targeted protein SCAP.

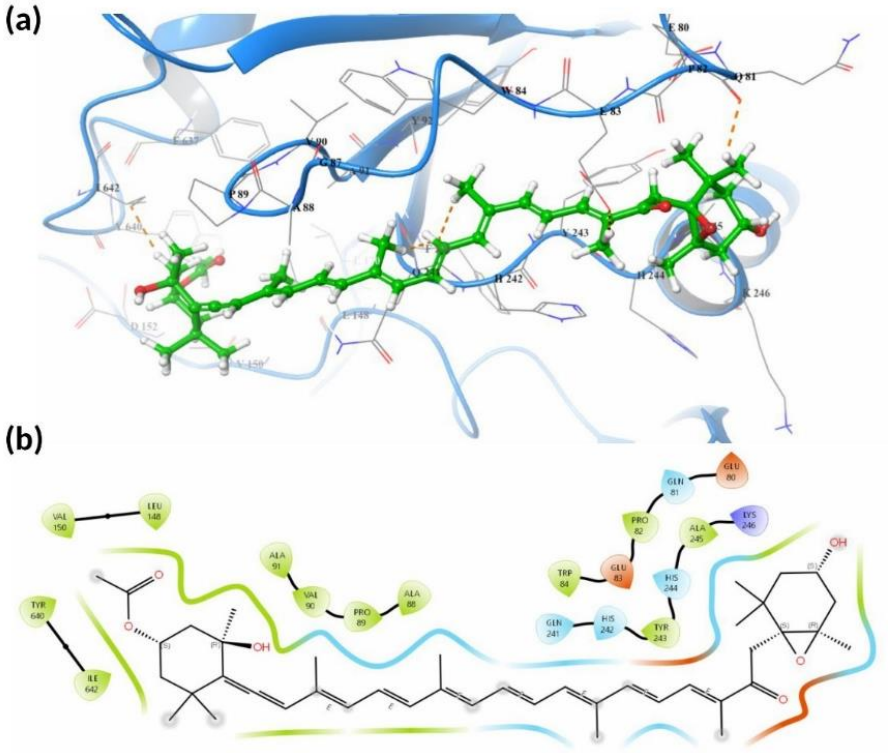

Figure 2. Molecular Docking Analysis of SCAP-Fucoxanthin (FX) binding interactions **(a)** Fucoxanthin (green) binding position inside the SCAP active site, interacting with the blue chain; **(b)** Schematic diagram illustrating key molecular interactions between SCAP and Fucoxanthin.

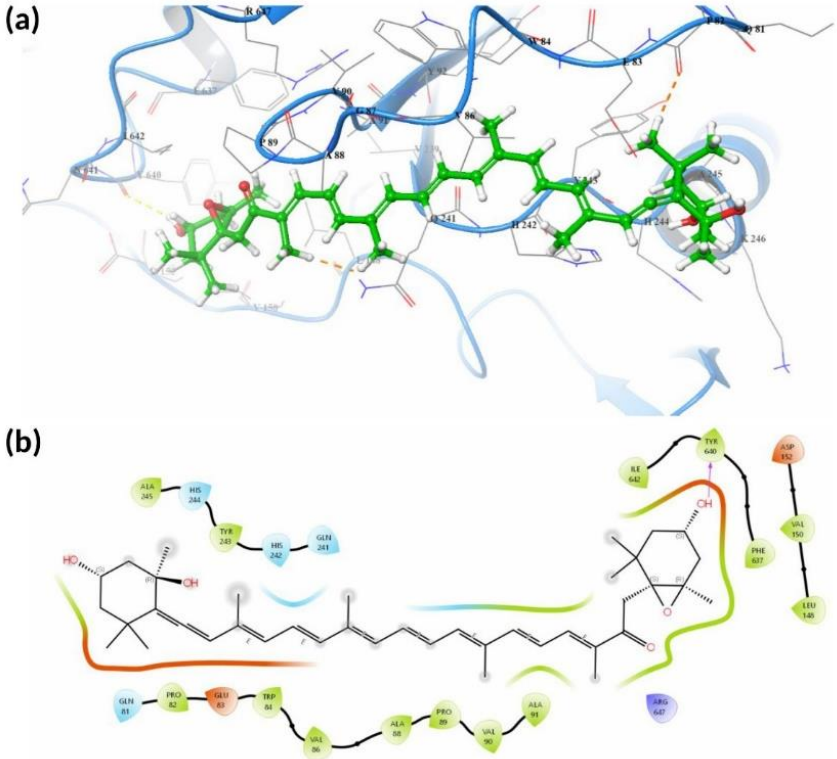

Figure 3. Molecular Docking Analysis of SCAP-Fucoxanthinol (FXOH) binding interaction **(a)** FXOH (green) binding position inside the SCAP active site, interacting with the blue chain; **(b)** Schematic diagram illustrating key molecular interactions between SCAP and Fucoxanthinol and hydrogen bond interaction (Pink) with Y640.

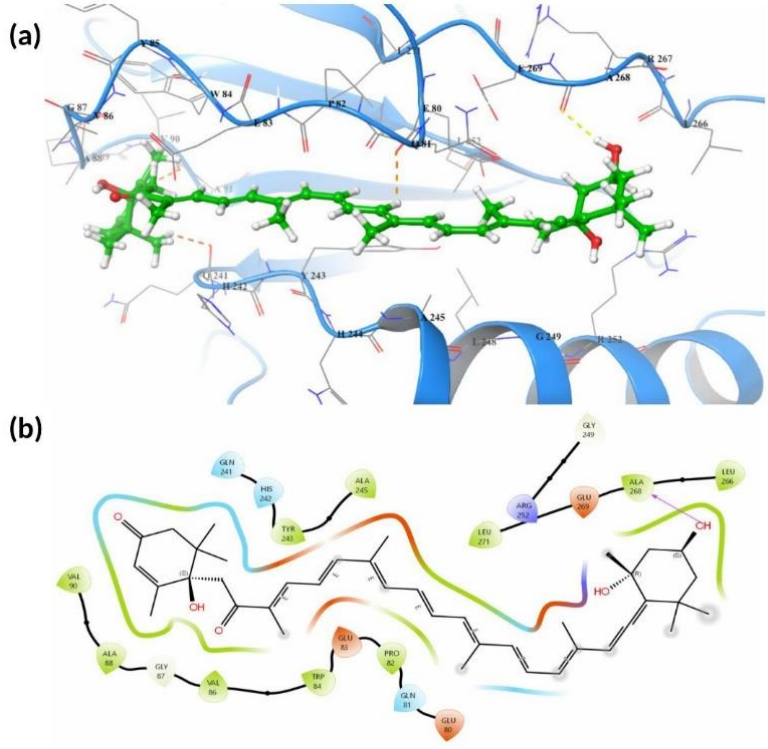

Figure 4. Molecular Docking Analysis of SCAP-Amarouciaxanthin A (AXA) binding interactions **(a)** AXA (green) binding position inside the SCAP active site, interacting with the blue chain; **(b)** Schematic diagram illustrating key molecular interactions between SCAP and Amarouciaxanthin A, and hydrogen bond interaction (Pink) with A268.

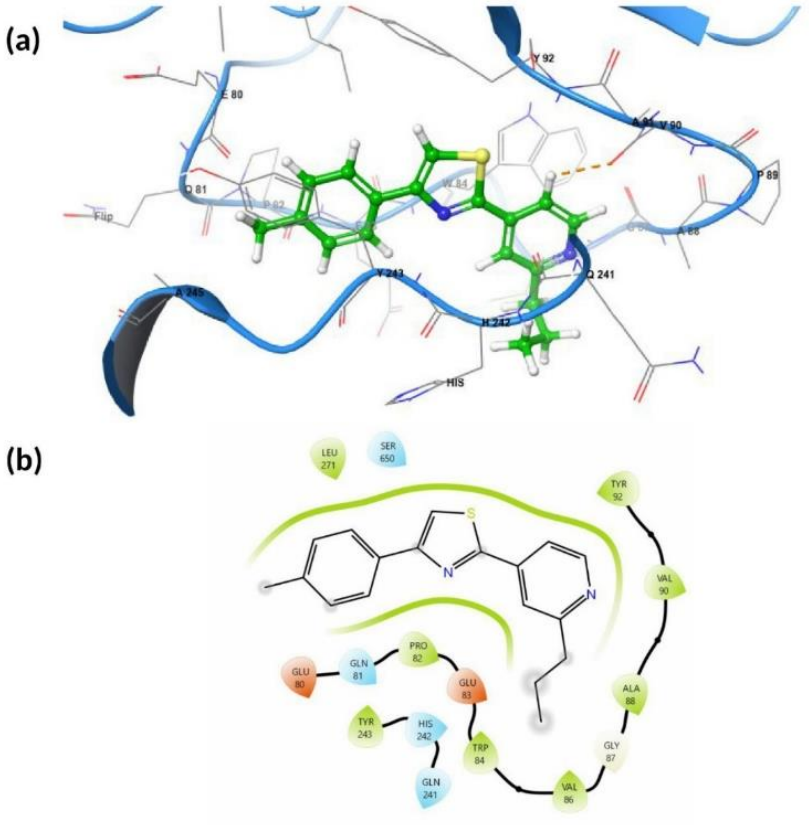

Figure 5. Molecular Docking Analysis of SCAP-Fatostatin binding interactions **(a)** Fatostatin (green) binding position inside the SCAP active site, interacting with the blue chain; **(b)** Schematic diagram illustrating key molecular interactions between SCAP and Fatostatin.

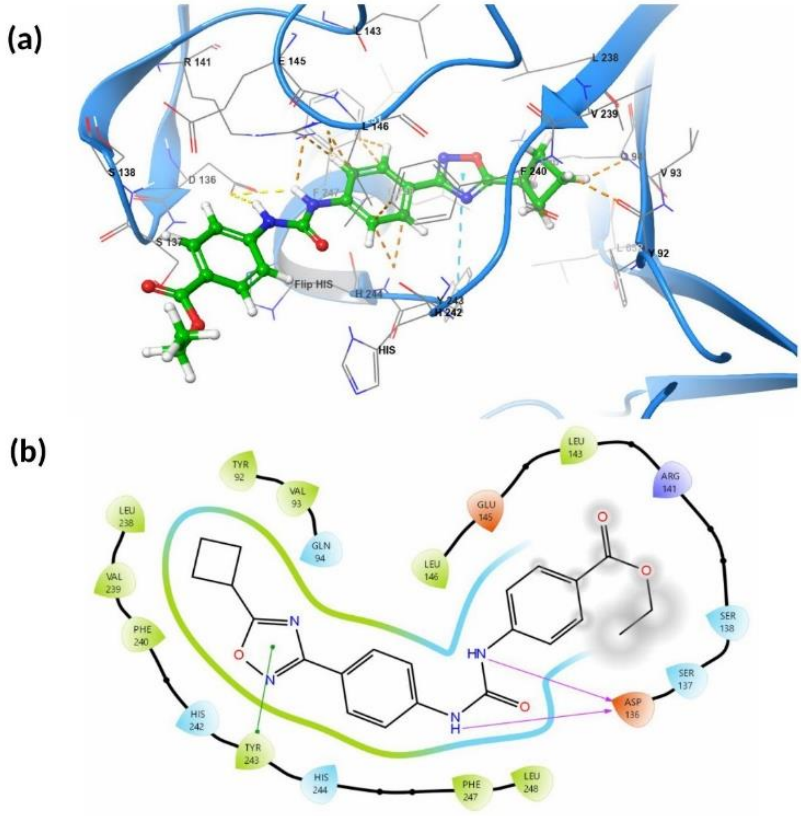

Figure 6. Molecular Docking Analysis of SCAP-UT-59 binding interactions **(a)** UT-59 (green) binding position inside the SCAP active site, interacting with the blue chain; **(b)** Schematic diagram illustrating key molecular interactions between SCAP and UT-59 and hydrogen bond interaction (Pink) with D136.

3.4. Molecular dynamics simulation (MDS).

3.4.1. Root mean square deviation (RMSD) analysis.

The structural stability of the SCAP-ligand complex was verified for 100 ns, and its molecular dynamics simulations were recorded in RMSD plots (Figure 8).

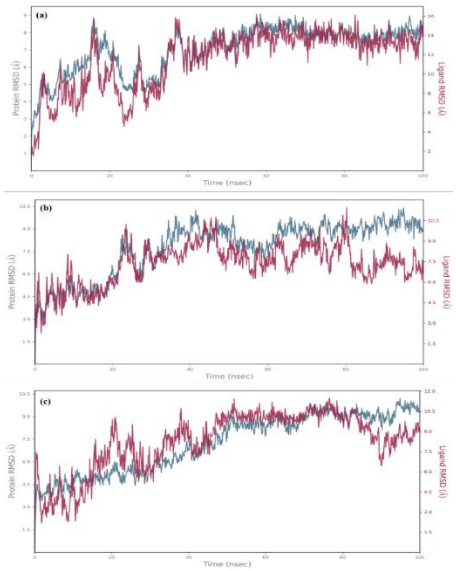

Figure 7. RMSD plot demonstrating the Protein-Ligand complex stability during a 100 ns period. The ligand RMSD (red, right Y-axis) and protein RMSD (blue, left Y-axis), which shows stability and variances in structure **(a)** SCAP-Fucoxanthin; **(b)** SCAP-Fucoxanthinol; (**c**) SCAP-Amarouciaxanthin A complex.

In the SCAP-FX complex, the protein maintained the RMSD values in the range of 7 Å to 9 Å after attaining equilibrium at 40 ns. The ligand FX maintained the RMSD values in the range of 13 Å to 15 Å after attaining equilibrium at 40 ns. This suggests that the ligand undergoes conformational changes, yet it fits well into the protein's active site, indicating the stability of the complex (Figure 8a). In the SCAP-FXOH complex, the protein maintained the RMSD values of ~ 9 Å after attaining equilibrium at 40 ns. The ligand FXOH maintained the RMSD values of ~ 7.5 Å after attaining equilibrium at 40 ns. This suggests that the ligand undergoes conformational changes, yet it fits well into the protein's active site, indicating the stability of the complex (Figure 8b). In the SCAP-AXA complex, the protein maintained the RMSD values between 9 Å and 10 Å after attaining equilibrium at 40 ns. The ligand (AXA) RMSD exhibited higher fluctuations, reaching 11 Å between 50 and 80 ns. After that, AXA maintained the RMSD values of 7.5 to 9 Å at 100 ns. This suggests that the ligand undergoes conformational changes, yet it fits well into the protein's active site, indicating the stability of the complex (Figure 8c).

3.4.2. Root mean square fluctuation (RMSF) analysis.

RMSF plots represent the fluctuations of protein and ligand atoms during simulation. In the SCAP-FX complex, the FX RMSF plot showed a high fluctuation at the atom positioned at C38 with 7 Å (Figure 9a). Protein RMSF analysis showed that most residues remained rigid, except for loop region residues ranging from 220 to 260, which exhibited fluctuation of ~ 8 Å (Figure 9b). A similar trend was observed in the SCAP-FXOH complex, where fucoxanthinol exhibited its highest at atom C2 with ~ 6.5 Å (Figure 10a), and the SCAP protein remained rigid, except for a loop region residue ranging from 220 to 260, whose values reached ~ 4.5 Å (Figure 10b). In the SCAP-AXA complex, Amarouciaxanthin A showed the highest fluctuation at the atom positioned at C2 with ~ 7 Å (Figure 11a). The SCAP protein maintains stability except for loop region residues ranging from 220 to 260, with the highest fluctuation ~ 6.5 Å (Figure 11b).

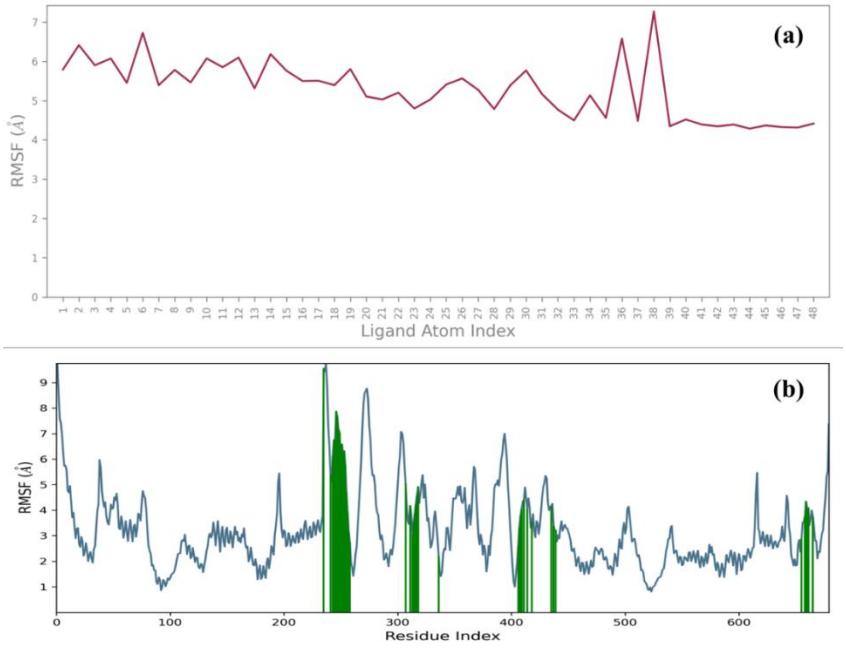

Figure 8. Root Mean Square Fluctuation (RMSF) graphs of ligand and protein **(a)** Fucoxanthin fit on protein; **(b)** Protein RMSF peaks indicate areas of the protein that fluctuate the most during the simulation. SCAP residues that interact with the FX are marked with green-coloured vertical bars.

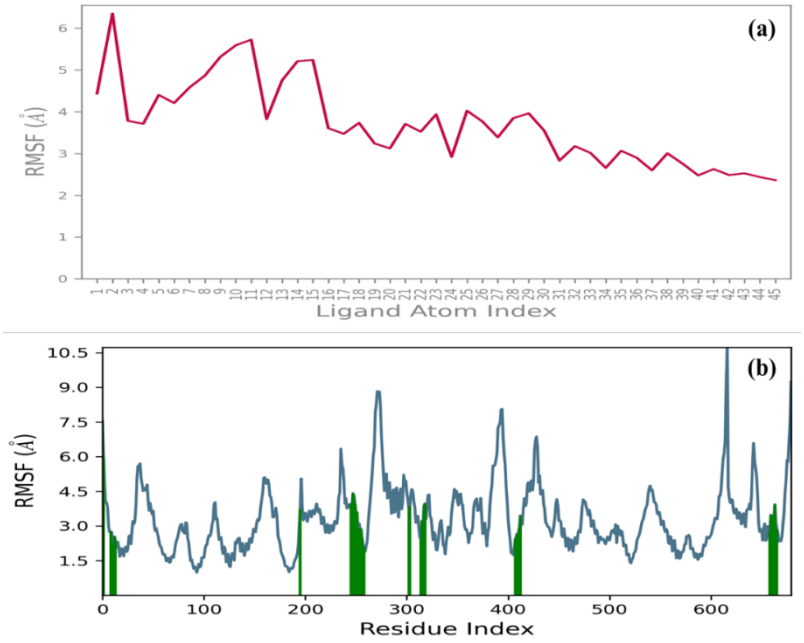

Figure 9. Root Mean Square Fluctuation (RMSF) graphs of ligand and protein **(a)** Fucoxanthinol fit on protein; **(b)** Protein RMSF peaks indicate areas of the protein that fluctuate the most during the simulation. SCAP residues that interact with the FXOH are marked with green-coloured vertical bars.

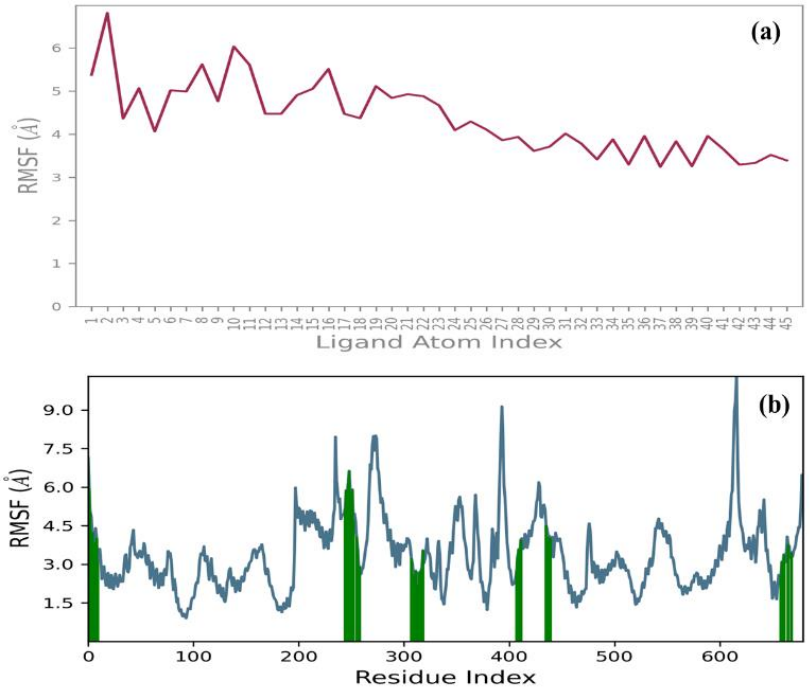

Figure 10. Root Mean Square Fluctuation (RMSF) graphs of ligand and protein **(a)** Amarouciaxanthin A fit on protein; **(b)** Protein RMSF peaks indicate areas of the protein that fluctuate the most during the simulation. SCAP residues that interact with the AXA are marked with green-coloured vertical bars.

3.4.3. Protein-ligand contacts.

The MDS revealed specific residues involved in hydrogen bonding for each SCAP-ligand complex. In the SCAP-FX complex, fucoxanthin (FX) showed hydrogen bonds with residues in chain B: PRO78, THR79, GLU80, GLN81, GLU83, TRP84, VLA86, ALA88, TRY92, GLN149, THR151, ASP152, GLN241, HIS242, TYR243, ARG252, HIS273, THR643, ARG647 (Figure 12a). In the SCAP-FXOH complex, fucoxanthinol (FXOH) formed hydrogen bonds in chain B, including GLU80, GLN81, PRO82, GLU83, TRP83, SER137,

GLN149, THR151, GLN241, TYR243, TYR640, ASN641, THR643, ARG647 (Figure 12 b). In the case of the SCAP-AXA complex, Amarouciaxanthin A (FXOH) formed hydrogen bonds with residues in chain B, including ARG141, GLU144, GLU145, GLN149, VLA150, THR151, ASP152, ASN641, and SER650 (Figure 12c). From MM-GBSA analysis, the binding energy of SCAP-FX complex had Coulombic energy (-16.23 kcal/mol), Covalent energy (-15.06 kcal/mol), Solvation (VSGB) was (37.17), Van der Waals energy contribution was (-10.45 kcal/mol), and total binding free energy of complex (-55.09 kcal/mol). Whereas the total binding free energies of SCAP-FXOH (-16.31 kcal/mol), SCAP-AXA (-35.86 kcal/mol), SCAP-fatostatin (-41.96 kcal/mol), and SCAP-UT-59 (-12.56 kcal/mol) (Table 5).

Table 5. Free binding energy calculation of SCAP-Ligand complexes.

Parameters	Ligands and Binding energy (kcal/mol)				
	Fucoxanthin (FX)	**Fucoxanthinol (FXOH)**	**Amarouciaxanthin A (AXA)**	**Fatostatin**	**UT-59**
Bind	-55.09	-16.31	-35.86	-41.96	-12.56
Coulomb	-16.23	-18.01	-18.08	-27.22	-17.14
Covalent	-15.06	42.89	35.33	4.13	46.68
Solv GB	37.17	62.80	-94.47	-9.34	5.62
vdW	-10.45	-32.22	-17.43	-16.90	-6.50

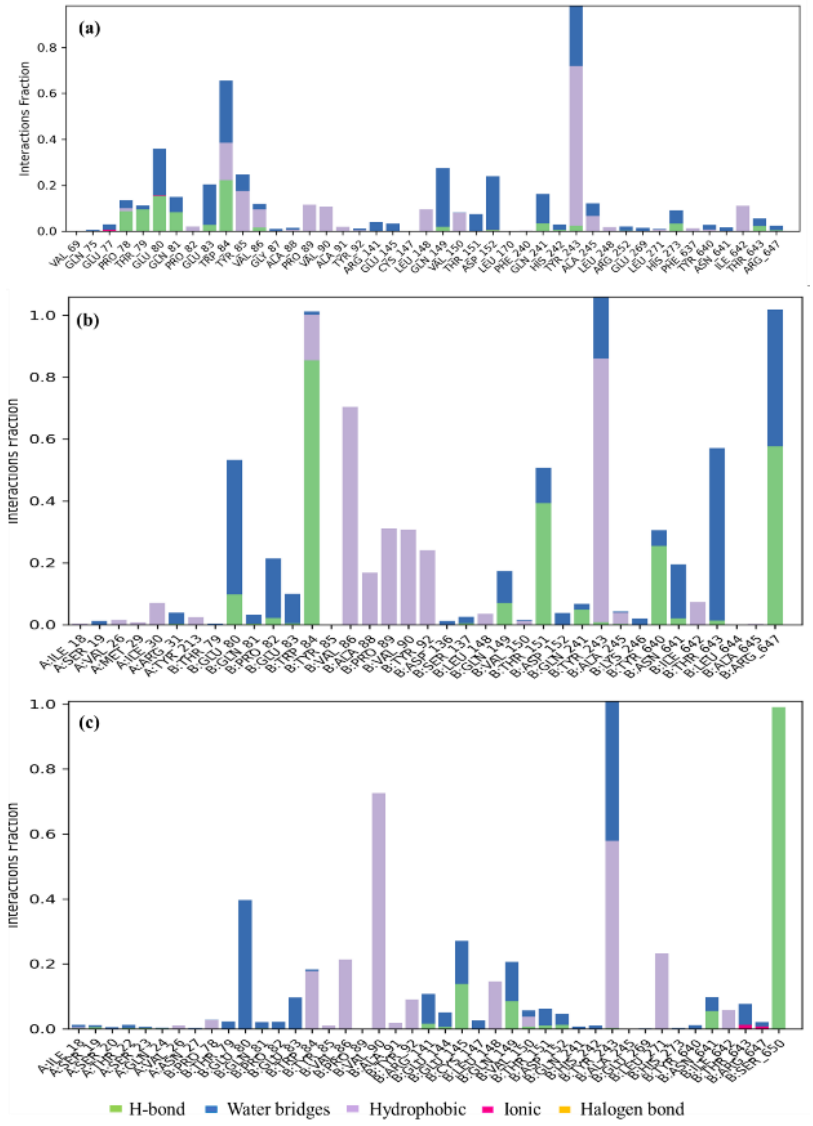

Figure 11. Protein-Ligand contacts **(a)** SCAP-Fucoxanthin; **(b)** SCAP-Fucoxanthinol; **(c)** SCAP-Amarouciaxanthin A complex.

4. Discussion

Fucoxanthin (FX) is a marine epoxyxanthophyll carotenoid found in brown algae. FX and its natural derivatives, such as fucoxanthinol (FXOH) and amarouciaxanthin A (AXA), contain long hydrocarbon chains, conjugated carbonyl groups, polyene structure, and oxygenic functional groups, including hydroxyl, epoxy, and carboxy moieties. Lipophilic compounds (Xanthophylls) can effectively diffuse through lipid bilayers and engage with hydrophobic binding sites inside membrane-bound receptors, ion channels, and transporters [22]. These features contribute to their high lipophilicity, increasing their membrane permeability and affinity for lipid-rich environments [23]. From the ADME prediction, fucoxanthin (FX) and its derivatives, FXOH and AXA, had lower water solubility and hydrophobicity than reference drugs (fatostatin and UT-59). The lipophilic compound can efficiently integrate into lipid bilayers, thereby improving the targeting efficiency of transmembrane proteins such as SCAP. Although computational ADME prediction can save expensive experimental procedures, it results in unnecessary testing of compounds that are bound to fail. Predicted ranges are provided using 95% of the known drugs.

Moreover, Protox prediction FX, FXOH, and AXA were Inactive for neurotoxicity, mutagenicity, cytotoxicity, cardiotoxicity, and hepatotoxicity as compared to fatostatin and UT-59. These results corresponded to the previous findings of Karpiński *et al*.; the pharmacokinetic parameters of xanthophylls predicted using SwissADME imply no AMES toxicity, hepatotoxicity, and skin permeability. The acute and chronic toxicity of xanthophylls in rats is comparable to that of control drugs. It is interesting that ivermectin and ritonavir exhibit hepatotoxicity. It indicates that xanthophylls are less harmful than these two medications approved by the FDA [36]. An *in vivo* experimental study found that a single oral administration of fucoxanthin (160 nmol) in mice led to the accumulation of metabolites fucoxanthinol (FXOH) and amarouciaxanthin A (AXA) in the adipose tissue, erythrocytes, kidneys, heart, liver, lungs, plasma, and spleen of all tested specimens. In contrast, FX (parent compound) was not found in any specimens [37]. Another study involving human volunteers reported that oral administration of fucoxanthin-enriched (31 mg) kombu (*Saccharina japonica*) extract led to FXOH concentration in plasma 44·2 nmol/l after 4 hours and 663·7 nmol/l after 24 h. These observations suggested that the bioavailability of fucoxanthin was lower than that of its metabolites [38]. The lipophilicity, high membrane diffusion, and low bioavailability of fucoxanthin and its derivatives enhance their therapeutic potential for lipid metabolic and neurological disorders [13,39–41]. However, its binding affinity and mode of interaction with SREBP cleavage-activating protein (SCAP) remain unclear. The current hypothesis provides insights into the binding affinities and interaction modes of FX, FXOH, and AXA with SCAP via molecular docking and molecular dynamics simulations, identifying key molecular interactions that contribute to their inhibitory potential.

Sterol regulatory element-binding factors (SREBFs) are a class of transcription factors, including SREBP1a, SREBP1c, and SREBP2, that are involved in lipid biosynthesis and play a critical role in the synthesis of SREB proteins. SREBPs can monitor cellular sterol levels by interacting with two membrane proteins, the insulin-induced gene 1 (INSIG and the SREBP cleavage-activating protein (SCAP) [20]. SCAP is a heterodimer peptide containing 1248 amino acids. SREBPs are stored as precursor forms in the endoplasmic reticulum (ER). In the presence of cholesterol, SCAP and SREBPs undergo conformational changes and form a stable complex with Insulin-induced gene 1 (INSIG1) to stay in the ER. The human SCAP/INSIG1

complex has a sterol-sensing domain (SSD) on the transmembrane segment of the SCAP [42,43].

The cryo-EM structure (PDB: 7ETW) reveals that SCAP promotes the activation and trafficking of SREBPs. SCAP contains eight transmembrane (TM) helices, whereas INSIG 2 has 6 helices. The majority of the loops in SCAP are short, except L6 (94 residues), L1 (239 residues), and L7 (176 residues). In INSIG1, all TM helices are linked by short loops. The SCAP-INSIG1 interaction is mostly mediated by TM helices, with minimal contacts between their cytosolic loops and few luminal interactions involving L1 and L7 [44]. SCAP protein characterization is essential to determine its structural morphology, identify new inhibitors [34], and proceed with structural characterization. A positive GRAVY value (0.022) suggests that more non-polar residues are present in SCAP, which are hydrophobic [35]. SCAP plays a crucial role in the prerequisite for transporting and activating all three SREBP isoforms. Targeting SREBPs seems to be an attractive strategy for treating metabolic diseases. Hence, this study predicted the SCAP inhibitory potential of natural marine-derived fucoxanthin and its derivatives using computational tools and compared it with synthetic drugs.

From docking analysis, the binding interactions of protein-ligands Amarouciaxanthin A exhibited the highest binding interaction (-7.543) with SCAP compared to FX (-4.175), FXOH (-4.853), fatostatin (-5.743), and UT-59 (-6.846). FX and fatostatin did not form hydrogen bonds with the targeted protein SCAP. While hydrogen bonding plays a crucial role in molecule recognition, poor binding does not always result from its absence. Even a ligand with significant electrostatic or hydrophobic interactions can have biological activity and a high binding affinity [45]. In a previous study, Shimeng *et al*. have identified UT-59, a small molecule that binds to the cholesterol-binding region of SCAP, which prevents SREBP activation and lipid synthesis [46].

The docked protein-ligand complexes were further validated using molecular dynamics (MD) simulations, which helped determine structural stability, binding efficiency, and protein-ligand interactions. After analyzing the MD simulation results, we observed that all complexes showed good stability throughout the simulation period (100 ns). RMSF revealed the difference between flexible and rigid regions in proteins. In contrast to loop areas, alpha helices and beta strands tend to be more rigid, whereas the N- and C-terminal tails typically show greater fluctuations. In the current study, we found that the SCAP protein remained structurally stable across all ligand complexes, with fluctuations primarily occurring in the loop region (220–260), while ligand flexibility varied, with FX and AXA exhibiting higher atomic fluctuations than FXOH. Protein-ligand contacts play a crucial role in molecular interactions within biological systems. Protein-ligand contacts are categorized into hydrogen bonds, hydrophobic, ionic, and water bridges. These contacts provide molecular specificity and stability to binding. MD simulation results confirm that the selected inhibitors bind effectively and remain stable within the active site, highlighting their potential efficacy.

5. Conclusions

Fucoxanthin (FX), a marine carotenoid, is metabolized into fucoxanthinol (FXOH) and amarouciaxanthin A (AXA) in the body. This study assessed their SCAP inhibitory potential using *in silico* methods, with fatostatin and UT-59 as reference drugs. ADME analysis revealed that all compounds were lipophilic, with low water solubility, high GI absorption, and low BBB permeability. AXA was predicted to be non-toxic, with no indications of hepatotoxicity, neurotoxicity, or mutagenicity. SiteMap identified a binding pocket in SCAP's luminal

domain. Docking results showed AXA had the strongest affinity (-7.543 kcal/mol), followed by UT-59 (-6.846), fatostatin (-5.743), FXOH (-4.853), and FX (-4.175). AXA formed a hydrogen bond with residue A268. Molecular dynamics (100 ns) confirmed stable complexes with RMSD 7.5-9 Å. MM-GBSA binding free energies supported favorable interactions for FX (-55.09 kcal/mol) and AXA (-35.86 kcal/mol). These findings suggest that AXA is a promising natural SCAP inhibitor and support its further evaluation through *in vitro* and *in vivo* studies for potential use as a cholesterol-lowering therapeutic agent.

Author Contributions

Conceptualization, S.B. and M.K.P.; methodology, S.B. and M.K.P.; software, T.S.K.P.; validation, S.B. and M.K.P.; formal analysis, S.B. and M.K.P.; investigation, S.B. and M.K.P.; resources, T.S.K.P.; data curation, S.B. and M.K.P.; writing—original draft preparation, S.B. and M.K.P.; writing—review and editing, T.S.K.P.; visualization, S.B. and M.K.P.; supervision, T.S.K.P.; All authors have read and agreed to the published version of the manuscript.

Institutional Review Board Statement

Not applicable.

Informed Consent Statement

Not applicable.

Data Availability Statement

Data supporting the findings of this study are available upon reasonable request from the corresponding author.

Funding

This research received no external funding.

Acknowledgments

The authors acknowledge the support of the Department of Biotechnology, Government of India, to the Yenepoya (Deemed to be University) through the project on “Skill Development in Mass Spectrometry-based metabolomics technology BIC” (BT/PR40202/BTIS/137/53/2023). We also thank the Indian Council of Medical Research (ICMR) for designating our Center as an ICMR-Collaborating Center of Excellence 2024 (ICMR-CCoE) in recognition of the commendable achievements in biomedical research.

Conflicts of Interest

The authors declare no conflict of interest.

Abbreviations

Abbreviation	Definition
AXA	Amarouciaxanthin A

Abbreviation	Definition
ADME	Absorption, Distribution, Metabolism, and Excretion
CNS	Central nervous system activity
Fx	Fucoxanthin
FXOH	Fucoxanthinol
MD	Molecular Docking
MDS	Molecular Dynamics Simulation
MM-GBSA	Molecular Mechanics Generalized Born Surface Area
NAFLD	Non-alcoholic fatty liver disease
RMSF	Root Mean Square Fluctuation
RMSD	Root Mean Square Deviation
SCAP	SREBP Cleavage-Activating Protein
SREBP	Sterol regulatory element-binding factors

References

1. Din, N.A.S.; Mohd Alayudin. A.S.; Sofian-Seng, N. S.; Rahman, H.A.; Mohd Razali, N.S.; Lim, S.J.; Wan Mustapha, W.A. Brown Algae as Functional Food Source of Fucoxanthin: A Review. *Foods* **2022**, *11*, 2235, https://doi.org/10.3390/foods11152235.
2. Anjana, K.; Arunkumar, K. Brown algae biomass for fucoxanthin, fucoidan and alginate; update review on structure, biosynthesis, biological activities and extraction valorisation. Int. J. Biol. Macromol. **2024**, *280*, 135632, https://doi.org/10.1016/J.IJBIOMAC.2024.135632.
3. Fariman, G.A.; Shastan, S.J.; Zahedi, M.M. Seasonal variation of total lipid, fatty acids, fucoxanthin content, and antioxidant properties of two tropical brown algae (Nizamuddinia zanardinii and Cystoseira indica) from Iran. *J. Appl. Phycol.* **2016**, *28*, 1323–1331, https://doi.org/10.1007/s10811-015-0645-y.
4. Mumu, M.; Das, A.; Emran, T.B.; Mitra, S.; Islam, F.; Roy, A.; Karim, M.M.; Das, R., Park, M.N.; Chandran, D.; Sharma, R. Fucoxanthin: A Promising Phytochemical on Diverse Pharmacological Targets. *Front. Pharmacol.* **2022**, *13*, 929442, https://doi.org/10.3389/fphar.2022.929442.
5. Miyashita, K.; Nishikawa, S.; Beppu, F.; Tsukui, T.; Abe, M.; Hosokawa, M. The allenic carotenoid fucoxanthin, a novel marine nutraceutical from brown seaweeds. *J. Sci. Food Agric.* **2011**, *91*, 1166–1174, https://doi.org/10.1002/jsfa.4353.
6. Paidi, M.K.; Attupuram, A.; Udata, K.S.; Mandal, S.K. Acetone diethyl ether-based biorefinery process for co-extraction of fucoxanthin, chlorophyll, DHA, and EPA from the diatom *Thalassiosira lundiana*. *Algal Res.* **2023**, *74*, 103215, https://doi.org/10.1016/j.algal.2023.103215.
7. Fung, A.; Hamid, N.; Lu, J. Fucoxanthin content and antioxidant properties of Undaria pinnatifida. *Food Chem.* **2013**, *136*, 1055–1062, https://doi.org/10.1016/j.foodchem.2012.09.024.
8. Neumann, U.; Derwenskus, F.; Flister, V.F.; Schmid-Staiger, U.; Hirth, T.; Bischoff, S.C. Fucoxanthin, a carotenoid derived from Phaeodactylum tricornutum exerts antiproliferative and antioxidant activities *in vitro*. *Antioxidants* **2019**, *8*, 183, https://doi.org/10.3390/antiox8060183.
9. Foo, S.C.; Khong, N.M.H.; Yusoff, F.M. Physicochemical, microstructure and antioxidant properties of microalgae-derived fucoxanthin rich microcapsules. *Algal Res.* **2020**, *51*, 102061, https://doi.org/10.1016/j.algal.2020.102061.
10. Sudhakar, M.P.; Ananthalakshmi, J.S.; Nair, B.B. Extraction, purification and study on antioxidant properties of fucoxanthin from brown seaweeds. *J. Chem. Pharm. Res.* **2013**, *5*, 169–175.
11. Maeda, H.; Hosokawa, M.; Sashima, T.; Funayama, K.; Miyashita, K. Fucoxanthin from edible seaweed, Undaria pinnatifida, shows anti-obesity effect through UCP1 expression in white adipose tissues. *Biochem. Biophys. Res. Commun.* **2005**, *332*, 392–397, https://doi.org/10.1016/J.BBRC.2005.05.002.
12. Maeda, H.; Kanno, S.; Kodate, M.; Hosokawa, M.; Miyashita, K. Fucoxanthinol, metabolite of fucoxanthin, improves obesity-induced inflammation in adipocyte cells. *Mar. Drugs* **2015**, *13*, 4799–4813, https://doi.org/10.3390/MD13084799.
13. Ye, J.; Zheng, J.; Tian, X.; Xu, B.; Yuan, F.; Wang, B.; Yang, Z.; Huang, F. Fucoxanthin Attenuates Free Fatty Acid-Induced Non-alcoholic Fatty Liver Disease by Regulating Lipid Metabolism/Oxidative Stress/Inflammation via the AMPK/Nrf2/TLR4 Signaling Pathway. *Mar. Drugs* **2022**, *20*, 225, https://doi.org/10.3390/md20040225.
14. Zhang, H.; Tang, Y.; Zhang, Y.; Zhang, S.; Qu, J.; Wang, X.; Kong, R.; Han, C.; Liu, Z. Fucoxanthin: A Promising Medicinal and Nutritional Ingredient. *Evid. Based Complement. Alternat. Med.* **2015**, *2015*, 723515, https://doi.org/10.1155/2015/723515.

15. Maeda, H.; Hosokawa, M.; Sashima, T.; Murakami-Funayama, K.; Miyashita, K. Anti-obesity and anti-diabetic effects of fucoxanthin on diet-induced obesity conditions in a murine model. *Mol. Med. Rep.* **2009**, *2*, 897–902, https://doi.org/10.3892/mmr_00000189.
16. Woo, M.N.; Jeon, S.M.; Kim, H.J.; Lee, M.K.; Shin, S.K.; Shin, Y.C.; Park, Y.B.; Choi, M.S. Fucoxanthin supplementation improves plasma and hepatic lipid metabolism and blood glucose concentration in high-fat fed C57BL/6N mice. *Chem. Biol. Interact.* **2010**, *186*, 316–322, https://doi.org/10.1016/j.cbi.2010.05.006.
17. Beppu, F.; Niwano, Y.; Sato, E.; Kohno, M.; Tsukui, T.; Hosokawa, M.; Miyashita, K. *In vitro* and in vivo evaluation of mutagenicity of fucoxanthin (FX) and its metabolite fucoxanthinol (FXOH). *J. Toxicol. Sci.* **2009**, *34*, 693–698, https://doi.org/10.2131/JTS.34.693.
18. Guo, B.; Oliviero, T.; Fogliano, V.; Ma, Y.; Chen, F.; Capuano, E. Gastrointestinal Bioaccessibility and Colonic Fermentation of Fucoxanthin from the Extract of the Microalga Nitzschia laevis. *J. Agric. Food Chem.* **2020,** *68*, 1844–1850, https://doi.org/10.1021/acs.jafc.9b02496.
19. Ha, A.W.; Kim, W.K. The effect of fucoxanthin rich power on the lipid metabolism in rats with a high fat diet. *Nutr. Res. Pract.* **2013**, *7*, 287–293, https://doi.org/10.4162/NRP.2013.7.4.287.
20. Shimano, H.; Sato, R. SREBP-regulated lipid metabolism: convergent physiology-divergent pathophysiology. *Nat. Rev. Endocrinol*. **2017,** *13*, 710–730, https://doi.org/10.1038/nrendo.2017.91.
21. Lee, S.H.; Lee, J.H.; Im, S.S. The cellular function of SCAP in metabolic signaling. *Exp. Mol. Med.* **2020**, *52*, 724–729, https://doi.org/10.1038/s12276-020-0430-0.
22. Zhu, Q.; Wang, S.; Fu, G.; Guo, F.; Huang, W.; Zhang, T.; Dong, H. Highly flexible cell membranes are the key to efficient production of lipophilic compounds. *J. Lipid Res.* **2024**, *65*, 100597, https://doi.org/10.1016/J.JLR.2024.100597.
23. Asai, A.; Yonekura, L.; Nagao, A. Low bioavailability of dietary epoxyxanthophylls in humans. *British J. Nutr.* **2008**, *100*, 273–277, https://doi.org/10.1017/S0007114507895468.
24. Høie, M.H.; Kiehl, E.N.; Petersen, B.; Nielsen, M.; Winther, O.; Nielsen, H.; Hallgren, J.; Marcatili, P. NetSurfP-3.0: accurate and fast prediction of protein structural features by protein language models and deep learning. *Nucleic Acids Res.* **2022**, *50*, W510-W515, https://doi.org/10.1093/NAR/GKAC439.
25. Falquet, L.; Pagni, M.; Bucher, P.; Hulo, N.; Sigrist, C.J.A.; Hofmann, K.; Bairoch, A. The PROSITE database, its status in 2002. *Nucleic Acids Res.* **2002**, *30*, 235–238, https://doi.org/10.1093/NAR/30.1.235.
26. Release Notes, Release 2024-4. Available online: https://www.schrodinger.com/life-science/download/release-notes/release-2024-4/.
27. SiteMap. Schrödinger. Available online: https://www.schrodinger.com/platform/products/sitemap/ (accessed on Day Month **Year**).
28. Glide. Available online: https://www.schrodinger.com/platform/products/glide/.
29. LigPrep. Available online: https://www.schrodinger.com/platform/products/ligprep/.
30. QikProp. Available online: https://www.schrodinger.com/platform/products/qikprop/.
31. Banerjee, P.; Kemmler, E.; Dunkel, M.; Preissner, R. ProTox 3.0: a webserver for the prediction of toxicity of chemicals. *Nucleic Acids Res.* **2024**, *52*, W513–W520, https://doi.org/10.1093/NAR/GKAE303.
32. Desmond. Available online: https://www.schrodinger.com/platform/products/desmond/.
33. Lu, C.; Wu, C.; Ghoreishi, D.; Chen, W.; Wang, L.; Damm, W.; Ross, G.A.; Dahlgren, M.K.; Russell, E.; Von Bargen, C.D.; Abel, R. OPLS4: Improving force field accuracy on challenging regimes of chemical space. *J. Chem. Theory Comput.* **2021**, *17*, 4291–4300, https://doi.org/10.1021/ACS.JCTC.1C00302.
34. Genheden, S.; Ryde, U. The MM/PBSA and MM/GBSA methods to estimate ligand-binding affinities. *Expert Opin. Drug Discov.* **2015**, *10*, 449-461, https://doi.org/10.1517/17460441.2015.1032936.
35. Prime. Available online: https://www.schrodinger.com/platform/products/prime/.
36. Karpiński, T.M.; Kwaśniewski, M.; Ozarowski, M.; Alam, R. *In silico* studies of selected xanthophylls as potential candidates against SARS-CoV-2 targeting main protease (Mpro) and papain-like protease (PLpro). *Herba Polonica* **2021**, *67*, 1–8, https://doi.org/10.2478/HEPO-2021-0009.
37. Hashimoto, T.; Ozaki, Y.; Mizuno, M.; Yoshida, M.; Nishitani, Y.; Azuma, T.; Komoto, A. Pharmacokinetics of fucoxanthinol in human plasma after the oral administration of kombu extract. *Br. J. Nutr.* **2012**, *107*, 1566–1569, https://doi.org/10.1017/S0007114511004879.
38. Hashimoto, T.; Ozaki, Y.; Taminato, M.; Das, S.K.; Mizuno, M.; Yoshimura, K.; Maoka, T.; Kanazawa, K. The distribution and accumulation of fucoxanthin and its metabolites after oral administration in mice. *Br. J. Nutr.* **2009**, *102*, 242–248, https://doi.org/10.1017/S0007114508199007.

39. Miyashita, K.; Beppu, F.; Hosokawa, M.; Liu, X.; Wang, S., Nutraceutical characteristics of the brown seaweed carotenoid fucoxanthin. *Arch. Biochem. Biophys.* **2020**, *686*, 108364, https://doi.org/10.1016/j.abb.2020.108364.
40. Asai, A.; Sugawara, T.;, Ono, H.; Nagao, A. Biotransformation of fucoxanthinol into amarouciaxanthin a in mice and HepG2 cells: Formation and cytotoxicity of fucoxanthin metabolites. *Drug Metab. Dispos.* **2004**, *32*, 205–211, https://doi.org/10.1124/dmd.32.2.205.
41. Martin, L.J. Fucoxanthin and its metabolite fucoxanthinol in cancer prevention and treatment. *Mar. Drugs* **2015**, *13*, 4784–4798, https://doi.org/10.3390/md13084784.
42. Yabe, D.; Brown, M.S.; Goldstein, J.L. Insig-2, a second endoplasmic reticulum protein that binds SCAP and blocks export of sterol regulatory element-binding proteins. *Proc. Natl. Acad. Sci. U.S.A.* **2002**, *99*, 12753–12758, https://doi.org/10.1073/pnas.162488899.
43. Horton, J.D.; Goldstein, J.L.; Brown, M.S. SREBPs: activators of the complete program of cholesterol and fatty acid synthesis in the liver. *J. Clin. Invest.* **2002**, *109*, 1125–1131, https://doi.org/10.1172/JCI0215593.
44. Yan, R.; Cao, P.; Song, W.; Li, Y.; Wang, T.; Qian, H.; Yan, C.; Yan, N. Structural basis for sterol sensing by Scap and Insig. *Cell Rep.* **2021**, *35*, 109299, https://doi.org/10.1016/j.celrep.2021.109299.
45. Chen, D.; Oezguen, N.; Urvil, P.; Ferguson, C.; Dann, S.M.; Savidge, T.C. Regulation of protein-ligand binding affinity by hydrogen bond pairing. *Sci. Adv.* **2016**, *2*, e1501240, https://doi.org/10.1126/SCIADV.1501240.
46. Xu, S.; Smothers, J.C.; Rye, D.; Endapally, S.; Chen, H.; Li, S.; Liang, G.; Kinnebrew, M.; Rohatgi, R.; Posner, B.A; Radhakrishnan, A. A cholesterol-binding bacterial toxin provides a strategy for identifying a specific Scap inhibitor that blocks lipid synthesis in animal cells. *Proc. Natl. Acad. Sci. U.S.A.* **2024**, *121*, e2318024121, https://doi.org/10.1073/PNAS.2318024121.

Publisher's Note & Disclaimer

Supplementary Materials

Table S1. Amino acid composition of SCAP protein.

Sl. No.	AA	Quantity	Percentage
1	Ala (A)	81	6.3%
2	Arg (R)	77	6.0%
3	Asn (N)	25	2.0%
4	Asp (D)	56	4.4%
5	Cys (C)	34	2.7%
6	Gln (Q)	46	3.6%
7	Glu (E)	65	5.1%
8	Gly (G)	106	8.3%
9	His (H)	31	2.4%
10	Ile (I)	59	4.6%
11	Leu (L)	165	12.9%
12	Lys (K)	35	2.7%
13	Met (M)	15	1.2%
14	Phe (F)	44	3.4%
15	Pro (P)	108	8.4%
16	Ser (S)	105	8.2%
17	Thr (T)	72	5.6%
18	Trp (W)	20	1.6%
19	Tyr (Y)	35	2.7%
20	Val (V)	100	7.8%
21	Pyl (O)	0	0.0%
22	Sec (U)	0	0.0%

Table S2. Physicochemical properties of SCAP protein.

Sl. No.	Physicochemical characteristics	Values
1	Number of amino acids	1279
2	Molecular weight	139729.03
3	Theoretical pI	6.41
4	Total number of negatively charged residues (Asp + Glu)	121
5	Total number of positively charged residues (Arg + Lys)	112
6	Total number of atoms	19743
7	Extinction coefficient	164275
8	Instability index	53.68
9	Aliphatic index	97.31
10	Grand average of hydropathicity (GRAVY)	0.022

Table S3. Domains and their positions are present in the SCAP protein.

Domain	Start	End	score
PS50156	284	442	43.285
PS50294	1075	1235	22.544
PS50082	1115	1155	12.547

Table S4. Experimental compounds or ligands and Simplified Molecular Input Line Entry System (SMILES).

Name of the Ligand	SMILES
Fucoxanthin	C/C(=C\C=C\C=C(/C)\C=C\C=C(/C)\C(=O)C[C@]12[C@](O1)(C[C@H](CC2(C)C)O)C)/C=C/C=C(\C)/C=C=C3[C@](C[C@H](CC3(C)C)OC(=O)C)(C)O
Fucoxanthinol	C/C(=C\C=C\C=C(/C)\C=C\C=C(/C)\C(=O)C[C@]12[C@](O1)(C[C@H](CC2(C)C)O)C)/C=C/C=C(\C)/C=C=C3[C@](C[C@H](CC3(C)C)O)(C)O
Amarouciaxanthin A	CC1=CC(=O)CC([C@]1(CC(=O)/C(=C/C=C/C(=C/C=C/C=C(\C)/C=C/C=C(\C)/C=C=C2[C@](C[C@H](CC2(C)C)O)(C)O)/C)/C)O)(C)C
Fatostatin	CCCC1=NC=CC(=C1)C2=NC(=CS2)C3=CC=C(C=C3)C
UT-59	CCOC(=O)C1=CC=C(NC(=O)NC2=CC=C(C3=NOC(C4CCC4)=N3)C=C2)C=C1

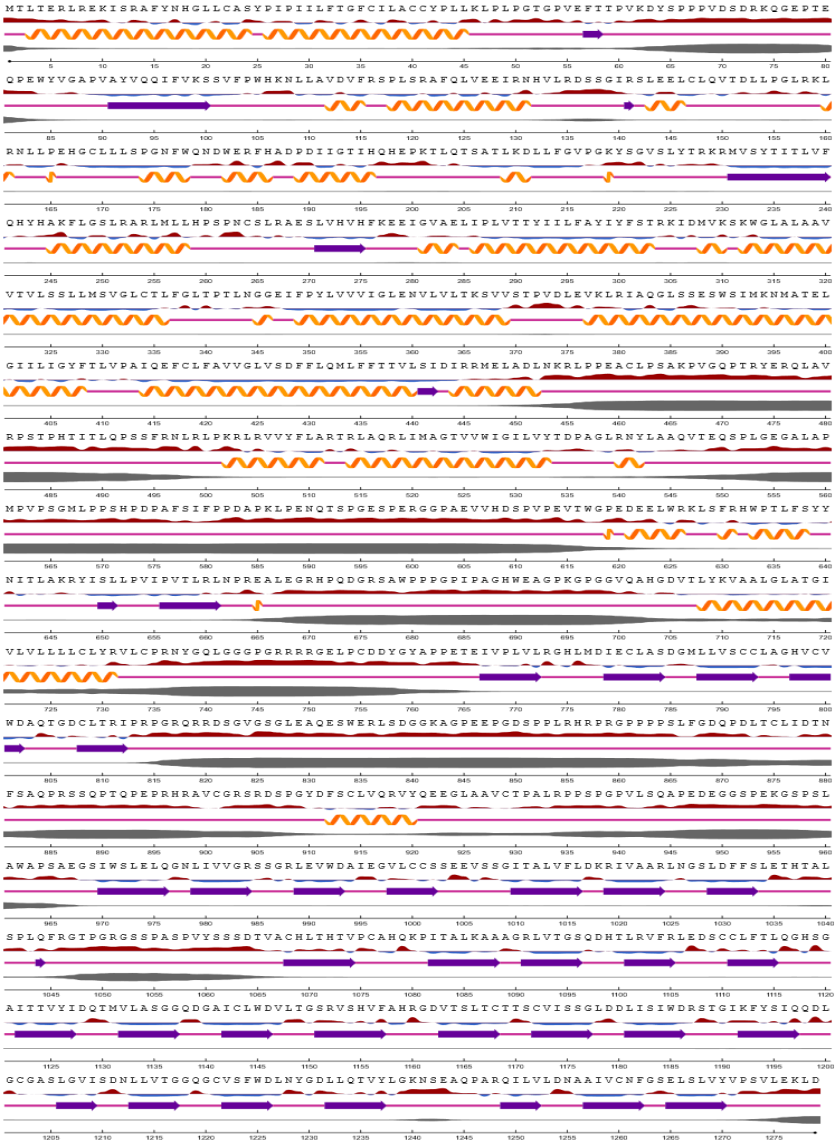

Figure S1. Secondary structure of the SCAP protein.